Distributed Formation Control for Unicycle Agents Using Fourier Descriptors

Miguel Aranda, Rodrigo Aldana-López, Eduardo Moya-Lasheras, Rosario Aragüés, and Carlos Sagüés

***Abstract*— This paper studies the control of multiagent formations in which the Fourier descriptors of the sequence of agent positions are constrained to be zero outside a selected set of low frequencies. This specification enables the mobile agents to form a low-frequency discretized planar closed curve without sharp variation while accommodating high flexibility of the curve's shape. We propose a novel approach for controlling this type of formation assuming a motion model with unicycle kinematics and velocity saturation. Our approach uses a distributed estimator to compute the values of the Fourier descriptors at the selected set of low frequencies, and employs these estimates in a gradient-based motion control strategy. We exploit existing techniques to define a convergent gradient-based control law under the considered motion constraints. Compared to prior work in this problem, our approach only requires distributed interactions between agents, and explicitly considers realistic motion constraints. We also study how to combine descriptors from different sets of frequencies, which enhances transient control performance. We present simulation examples to illustrate the properties of the proposed approach.**

I. Introduction

In a number of application scenarios involving multiagent systems, it is beneficial for the agents to deploy themselves according to a prescribed geometric configuration, called a formation. Such scenarios include object transport, area monitoring, or enclosing of dynamic phenomena [1], [2]. Commonly, formations are specified and controlled using interagent relative quantities such as distances [3], [4], positions [5], [6], or bearings [7], [8]. Advantages can be gained by exploiting formation control designs based on multiple layers [9], [10], or by using lower-dimensional formation specifications. Examples of the latter include fitting into a concentration ellipse [11], satisfying geometric moment statistics [12], aggregating in a polytope [13], or conforming to a desired density profile in a ring [14].

A previous formation control study [15] proposed arranging the sequence of positions of the agents in a team, according to a given order, in a discretized planar closed curve whose Fourier descriptors are allowed to be non-zero only for a selected set of low discrete frequencies. This way, the formed curves have a smooth and, at the same time, highly flexible shape, making them well suited for tasks such as target enclosing. The Fourier formalism for curve representation was also exploited in studies [16], [17], which focused on fitting a multiagent team to a specific boundary in the workspace. In contrast, the approach in [15] aimed to avoid constraining the specific shape of the curve, thus keeping it more adaptable to task demands. In this paper, we build on [15], presenting novel additions as detailed next.

To improve in scalability, we propose an estimator-based control approach that requires only distributed interactions, via communication, between agents. The use of estimators in multiagent formation control is a common approach [10], [12], [18]. Here, we apply a finite-time-convergent dynamic average consensus algorithm based on [19] to estimate the Fourier descriptors for the selected set of low frequencies. Regarding the motion control, while [15] assumed integrator dynamics, here we design a new strategy for agents with unicycle kinematics and saturated velocities. Concretely, we exploit a gradient-based control law so that the agents can reach a discretized curve with only low-frequency Fourier descriptors. This control law can be implemented by each agent using its current estimates of these Fourier descriptors and is initially designed for single-integrator dynamics. Then, we adapt it to unicycles with saturated velocities following the methodology in [20], while preserving the global convergence to the desired type of curve.

Our contributions over [15] are: 1) an estimator-based control approach requiring only distributed agent interactions, which is more easily scalable for teams with many agents; 2) a control law for agents with unicycle kinematics and saturated velocities, which increases applicability on real-world platforms; and additionally 3) a method for combining multiple sets of low frequencies, which allows controlling the frequency content during the transient interval.

Overall, our approach allows the agents to form a low-frequency discretized closed curve. This avoids sharp variation, tending to preserve the physical vicinity of neighboring agents along the sequence. Moreover, compared to standard formation control approaches [3], [4], [5], [6], [7], [8] where a team can achieve shapes equal to a nominal one up to prescribed types of transformation (e.g., translational, rigid, or affine), with the Fourier representation used here the shapes for the formed curve are not tied to a nominal shape. This makes it possible to achieve more flexible shapes. We illustrate these features of our approach, which are useful for enclosing tasks, with simulation examples.

This work was supported by MCIN/AEI/10.13039/501100011033, by ERDF A way of making Europe and by the European Union NextGenerationEU/PRTR under projects PID2021-124137OB-I00 and TED2021-130224B-I00, by the Universidad de Zaragoza and Banco Santander, by the Consejo Nacional de Ciencia y Tecnología (CONACYT-Mexico) with grant number 739841, and through a María Zambrano Fellowship funded by the Spanish Ministry of Universities and the European Union-NextGenerationEU.

The authors are with the Instituto de Investigación en Ingeniería de Aragón (I3A), Universidad de Zaragoza, Zaragoza 50018, Spain. Email: miguel.aranda@unizar.es, rodrigo.aldana.lopez@gmail.com, emoya@unizar.es, raragues@unizar.es, csagues@unizar.es.

This is the author's version of an article published in the proceedings of the 2024 IEEE 63rd Conference on Decision and Control (CDC).
The publisher's version and the citation information are available at https://doi.org/10.1109/CDC56724.2024.10886316

A. Notation

We use $\mathbf{I}_n$ to denote the $n \times n$ identity matrix. We denote the Euclidean norm of a vector or the spectral norm of a matrix by $\|\cdot\|$, and the infinity norm of a vector by $\|\cdot\|_\infty$. We denote ordered sequences by $(\cdot)$, and unordered sets by $\{\cdot\}$. By $\text{sgn}(\mathbf{x})$ where $\mathbf{x}$ is an array of real numbers we denote the component-wise signum function. For a vector field $\mathbf{f}(\mathbf{x})$, $\partial\mathbf{f}/\partial\mathbf{x}$ denotes its Jacobian. For a scalar field $f(\mathbf{x})$, $\nabla_\mathbf{x} f = (\partial f/\partial \mathbf{x})^\intercal$ denotes its gradient.

II. Problem formulation

Consider N mobile agents (where $N \geq 4$) in a planar environment, each having a different index in the set $\mathcal{N} = \{0, 1, \ldots, N-1\}$. The first index is taken to be 0 instead of 1 for notational convenience. We assume these indices are fixed and pre-assigned, and every agent knows its own index. The indices define an ordering of the agents in the following sequence: $(0, 1, \ldots, N-1)$. We take $t = 0$ as the initial time instant. For every agent $i \in \mathcal{N}$, we denote its position in a fixed absolute Cartesian coordinate system by $\mathbf{p}_i(t) = [x_i(t), y_i(t)]^\intercal \in \mathbb{R}^2$. We assume the agents move according to the unicycle model. For this, we denote by $\theta_i(t) \in \mathbb{R}$ for every agent i its heading angle measured counterclockwise relative to the direction of the positive x-axis. $v_i(t) \in \mathbb{R}$ denotes agent i's linear velocity, which produces a displacement aligned with its heading. $\omega_i(t) \in \mathbb{R}$ denotes the agent's angular velocity, positive in the counterclockwise (i.e., left-turn) direction. The dynamics under the considered unicycle model have the form:

$$\begin{aligned} \dot{x}_i(t) &= v_i(t)\cos(\theta_i(t)), \\ \dot{y}_i(t) &= v_i(t)\sin(\theta_i(t)), \\ \dot{\theta}_i(t) &= \omega_i(t). \end{aligned} \tag{1}$$

The functions $v_i(t)$ and $\omega_i(t)$ $\forall i \in \mathcal{N}$ are assumed to be measurable and bounded by saturation constraints: concretely, similarly to [20], for all $t \geq 0$ the velocities satisfy

$$-v_{b_i} \leq v_i(t) \leq v_{f_i}, \;\; -\omega_{r_i} \leq \omega_i(t) \leq \omega_{l_i}, \tag{2}$$

where $v_{f_i} > 0$, $v_{b_i} > 0$ are respectively the maximum forward and backward speed, while $\omega_{l_i} > 0$ and $\omega_{r_i} > 0$ are respectively the maximum left-turn and right-turn speed. We define $v_{\max} = \max\{v_{f_0}, v_{b_0}, \ldots, v_{f_{N-1}}, v_{b_{N-1}}\}$. The saturation constraints can be written using the following auxiliary functions for linear and angular velocities v, ω:

$$\text{sat}_{v_i}(v) = \begin{cases} -v_{b_i}, & v \in (-\infty, -v_{b_i}) \\ v, & v \in [-v_{b_i}, v_{f_i}] \\ v_{f_i}, & v \in (v_{f_i}, +\infty) \end{cases}, \tag{3}$$

$$\text{sat}_{\omega_i}(\omega) = \begin{cases} -\omega_{r_i}, & \omega \in (-\infty, -\omega_{r_i}) \\ \omega, & \omega \in [-\omega_{r_i}, \omega_{l_i}] \\ \omega_{l_i}, & \omega \in (\omega_{l_i}, +\infty) \end{cases}. \tag{4}$$

We assume every agent i knows its current position $\mathbf{p}_i(t)$ and heading $\theta_i(t)$, and agents can communicate to exchange data. The available communication structure is modeled via a simple undirected graph $\mathcal{G} = (\mathcal{N}, \mathcal{E})$ where $\mathcal{N}$ is the set of nodes, each corresponding to an agent, and $\mathcal{E} \subset \mathcal{N} \times \mathcal{N}$ is the set of edges, each of which is a pair (i, j) that represents the fact that node i can receive data from node j. As $\mathcal{G}$ is undirected, $(i, j) \in \mathcal{E} \Leftrightarrow (j, i) \in \mathcal{E}$. We then say that nodes (equivalently, agents) i and j are graph neighbors. We denote by $\mathcal{N}_i \subset \mathcal{N}$ the set containing the indices of the agents that are graph neighbors of i in $\mathcal{G}$. We assume that the graph $\mathcal{G}$ is time-invariant and connected.

A. Representing configurations with Fourier descriptors

In this section, we focus on the geometric properties of the ordered sequence of 2-D agent positions at time instant t, defined as $\mathtt{P}(t) = (\mathbf{p}_0(t), \ldots, \mathbf{p}_{N-1}(t))$. We use the discrete Fourier transform (DFT) [21, Ch. 5], a well-known frequency-domain representation that can be exploited for representing planar curves [15], [17], [22], [23]. For this, $x_i(t)$ and $y_i(t)$ for each i at t are interpreted as, respectively, the real and imaginary parts of a complex number. Here, we equivalently express the DFT with real numbers. Let us define the rotation matrix

$$\mathbf{R}(l) = \begin{bmatrix} \cos(-2\pi l/N) & -\sin(-2\pi l/N) \\ \sin(-2\pi l/N) & \cos(-2\pi l/N) \end{bmatrix}, \tag{5}$$

for arbitrary natural number l, and angles expressed in radians. Note $\mathbf{R}(0) = \mathbf{I}_2$. Then, the DFT of $\mathtt{P}(t)$ is the sequence $\mathtt{D}(t) = (\mathbf{d}_0(t), \ldots, \mathbf{d}_{N-1}(t))$ where

$$\mathbf{d}_k(t) = \sum_{i=0}^{N-1} \mathbf{R}(k \cdot i)\, \mathbf{p}_i(t), \quad k = 0, 1, \ldots, N-1. \tag{6}$$

Note that the transform is applied over the agent indices i, parameterizing the spatial curve that the agents form at a given time instant t. We refer to the N elements of $\mathtt{D}(t)$ as the Fourier descriptors of $\mathtt{P}(t)$ [22, Ch. 11]. We will often call them simply descriptors in this paper, for brevity. The index $k \in \mathcal{N}$ of descriptor $\mathbf{d}_k(t) \in \mathbb{R}^2$ represents a discrete spatial frequency value, equal to k cycles per N spatial points. The inverse DFT (IDFT) [15], [22] of the sequence $\mathtt{D}(t)$ returns the sequence $\mathtt{P}(t)$ and is defined as

$$\mathbf{p}_i(t) = \frac{1}{N} \sum_{k=0}^{N-1} \mathbf{R}(k \cdot i)^\intercal\, \mathbf{d}_k(t), \quad i = 0, 1, \ldots, N-1. \tag{7}$$

We represent the DFT as a linear transformation [21, Ch. 5], as done in [15]. For this purpose, we represent the sequences $\mathtt{P}(t)$, $\mathtt{D}(t)$ equivalently as the column vectors $\mathbf{p}(t) = [\mathbf{p}_0(t)^\intercal, \ldots, \mathbf{p}_{N-1}(t)^\intercal]^\intercal \in \mathbb{R}^{2N}$ and $\mathbf{d}(t) = [\mathbf{d}_0(t)^\intercal, \ldots, \mathbf{d}_{N-1}(t)^\intercal]^\intercal \in \mathbb{R}^{2N}$, which allows one to write:

$$\mathbf{d}(t) = \mathbf{M}\mathbf{p}(t), \;\; \mathbf{p}(t) = \mathbf{M}^{-1}\mathbf{d}(t), \tag{8}$$

where $\mathbf{M}$ is a fixed real matrix with size $2N \times 2N$ that has the following form:

$$\mathbf{M} = \begin{bmatrix} \mathbf{I}_2 & \mathbf{I}_2 & \mathbf{I}_2 & \cdots & \mathbf{I}_2 \\ \mathbf{I}_2 & \mathbf{R}(1) & \mathbf{R}(2) & \cdots & \mathbf{R}(N-1) \\ \mathbf{I}_2 & \mathbf{R}(2) & \mathbf{R}(4) & \cdots & \mathbf{R}(2(N-1)) \\ \vdots & \vdots & \vdots & \ddots & \vdots \\ \mathbf{I}_2 & \mathbf{R}(N-1) & \mathbf{R}(2(N-1)) & \cdots & \mathbf{R}((N-1)(N-1)) \end{bmatrix} \tag{9}$$

and whose inverse has the form $\mathbf{M}^{-1} = (1/N)\mathbf{M}^\intercal$.

B. Formation specification based on Fourier descriptors

Any sequence of agent positions $\mathtt{P}(t)$, represented as $\mathbf{p}(t)$, can be interpreted as a discretized planar closed curve. The DFT $\mathbf{d}(t)$ represents the frequency content of this curve with a descriptor at each frequency. High frequencies correspond to sharp variation and local detail in the curve [22, Ch. 11]. Following [15], our idea is to continuously drive $\mathbf{p}(t)$ toward a configuration with descriptors equal to zero outside a selected set of low frequencies. This will avoid sharp variation while allowing for flexible configurations, which is interesting, e.g., for enclosing tasks. Let us first define H as the fixed odd number, $3 \leq H < N$, of low frequencies to be used. Then, our set of H selected low frequencies, which correspond to the indices of the DFT $\mathbf{d}(t)$, is defined as

$$\mathcal{H} = \{0, 1, \ldots, (H-1)/2, N-(H-1)/2, \ldots, N-1\}. \quad (10)$$

Since frequencies k and $k-N$ are equivalent (note $\mathbf{R}(k\cdot i) = \mathbf{R}((k-N)\cdot i)$ in (6)), $\mathcal{H}$ contains positive and negative low frequencies lying symmetrically around the zero frequency.

For a given $\mathbf{p}(t) \in \mathbb{R}^{2N}$, we consider the configuration having the same descriptors as $\mathbf{p}(t)$ for the frequencies in $\mathcal{H}$, and descriptors with value zero for the frequencies outside $\mathcal{H}$. We call this configuration $\mathbf{p}_\mathcal{H}(t) \in \mathbb{R}^{2N}$. As seen in [15, Sec. II.C], the sequence of positions in $\mathbf{p}_\mathcal{H}(t)$ forms a discretized curve obtained by evenly sampling the angular parameter of a continuous closed parametric curve consisting of a sum of sinusoids for the frequencies in $\mathcal{H}$. If one chooses $H = 3$, $\mathbf{p}_\mathcal{H}(t)$ is a discretized ellipse. With $H > 3$, $\mathbf{p}_\mathcal{H}(t)$ can have a more flexible shape while still remaining low-frequency. Figure 1 shows two illustrative examples for $N = 7$.

Let us now describe how to obtain $\mathbf{p}_\mathcal{H}(t)$. We rewrite $\mathbf{M}$ in (9) as composed of $N \times N$ blocks $\mathbf{M}_{i,j}$ of size 2×2 as

$$\mathbf{M} = \begin{bmatrix} \mathbf{M}_{0,0} & \mathbf{M}_{0,1} & \cdots & \mathbf{M}_{0,N-1} \\ \mathbf{M}_{1,0} & \mathbf{M}_{1,1} & \cdots & \mathbf{M}_{1,N-1} \\ \vdots & \vdots & \ddots & \vdots \\ \mathbf{M}_{N-1,0} & \mathbf{M}_{N-1,1} & \cdots & \mathbf{M}_{N-1,N-1} \end{bmatrix}. \quad (11)$$

Then, we define

$$\mathbf{M}_\mathcal{H} = \begin{bmatrix} \mathbf{M}_{0,0} & \mathbf{M}_{0,1} & \cdots & \mathbf{M}_{0,N-1} \\ \vdots & \vdots & \ddots & \vdots \\ \mathbf{M}_{\frac{H-1}{2},0} & \mathbf{M}_{\frac{H-1}{2},1} & \cdots & \mathbf{M}_{\frac{H-1}{2},N-1} \\ \mathbf{M}_{N-\frac{H-1}{2},0} & \mathbf{M}_{N-\frac{H-1}{2},1} & \cdots & \mathbf{M}_{N-\frac{H-1}{2},N-1} \\ \vdots & \vdots & \ddots & \vdots \\ \mathbf{M}_{N-1,0} & \mathbf{M}_{N-1,1} & \cdots & \mathbf{M}_{N-1,N-1} \end{bmatrix} \quad (12)$$

which has size $2H \times 2N$ and contains the rows of $\mathbf{M}$ corresponding to the frequencies in $\mathcal{H}$. We can now define

$$\mathbf{d}_\mathcal{H}(t) = \mathbf{M}_\mathcal{H}\mathbf{p}(t) \quad \in \mathbb{R}^{2H} \quad (13)$$

which contains the descriptors of $\mathbf{p}(t)$ for frequencies in $\mathcal{H}$, following (8). As $\mathbf{p}_\mathcal{H}(t)$ has descriptors $\mathbf{d}_\mathcal{H}(t)$ for the frequencies in $\mathcal{H}$ and zero for all other frequencies, we just need to consider the columns of the inverse transform matrix $\mathbf{M}^{-1} = (1/N)\mathbf{M}^\intercal$ for frequencies in $\mathcal{H}$, having

$$\mathbf{p}_\mathcal{H}(t) = (1/N)\mathbf{M}_\mathcal{H}^\intercal \mathbf{d}_\mathcal{H}(t) = (1/N)\mathbf{M}_\mathcal{H}^\intercal \mathbf{M}_\mathcal{H}\mathbf{p}(t) = \mathbf{A}\mathbf{p}(t), \quad (14)$$

where we define the matrix $\mathbf{A} = (1/N)\mathbf{M}_\mathcal{H}^\intercal \mathbf{M}_\mathcal{H} \in \mathbb{R}^{2N\times 2N}$. This matrix was already used in [15] and is presented here in an alternative form more fitting for our formulation. Hence, $\mathbf{p}_\mathcal{H}(t)$ can be interpreted as a projection by the matrix $\mathbf{A}$ which is symmetric, positive semidefinite and idempotent.

We call the configuration

$$\mathbf{p}_\mathcal{H}(t) = [\mathbf{p}_{\mathcal{H},0}(t)^\intercal, \ldots, \mathbf{p}_{\mathcal{H},N-1}(t)^\intercal]^\intercal \quad (15)$$

the desired formation at time t, and we call $\mathbf{p}_{\mathcal{H},i}(t) \in \mathbb{R}^2$ the desired position for agent i at time t. Notice that for agent i

$$\mathbf{p}_{\mathcal{H},i}(t) = \frac{1}{N}\left[\mathbf{M}_{0,i}, \ldots, \mathbf{M}_{\frac{H-1}{2},i}, \mathbf{M}_{N-\frac{H-1}{2},i}, \ldots, \mathbf{M}_{N-1,i}\right] \mathbf{d}_\mathcal{H}(t). \quad (16)$$

The problem we address in this work consists in designing, under the described conditions, a multiagent control law such that the team reaches the desired formation: i.e., the positions of the agents satisfy $\mathbf{p}(t) \to \mathbf{p}_\mathcal{H}(t)$ as $t \to \infty$.

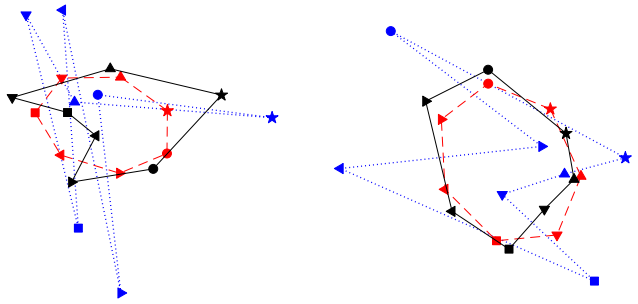

Fig. 1. Two examples (left and right) with $N = 7$. Agent positions are shown with different markers, and neighbors according to the sequence are joined by lines. In both examples, the configurations shown are $\mathbf{p}$ (blue, dotted lines), $\mathbf{p}_\mathcal{H}$ with $H = 5$, i.e., $\mathcal{H} = \{0, 1, 2, 5, 6\}$ (black, solid lines), and $\mathbf{p}_\mathcal{H}$ with $H = 3$, i.e., $\mathcal{H} = \{0, 1, 6\}$ (red, dashed lines).

III. Proposed estimator-controller strategy

Our strategy for solving the stated problem combines an estimator and a controller. Concretely, every agent i will obtain an estimate of $\mathbf{d}_\mathcal{H}(t)$ via a distributed consensus algorithm and use this to estimate its desired position $\mathbf{p}_{\mathcal{H},i}(t)$ according to (16) and, simultaneously, the agent will run a motion controller to move toward its desired position.

A. Distributed estimation of descriptors

In our proposed scheme, every agent estimates the vector $\mathbf{d}_\mathcal{H}(t)$, which contains the descriptors for the frequencies in $\mathcal{H}$. For this purpose, we exploit the fact that the DFT has a linear structure. This allows us to estimate $\mathbf{d}_\mathcal{H}(t)$ by means of an average consensus algorithm, using properly defined reference signals at each agent as a function of its current position. Since the agents are moving, we need to use an algorithm capable of handling time-varying reference signals. We propose to use the dynamic average consensus

algorithm in [19, eq. 1], which is also discussed in [24] and is sliding-mode-based. For every agent $i \in \mathcal{N}$ we define a vector $\hat{\mathbf{d}}_{\mathcal{H}}^{(i)}(t) \in \mathbb{R}^{2H}$ containing its local estimate of $\mathbf{d}_{\mathcal{H}}(t)$. The algorithm for every agent $i \in \mathcal{N}$ has the following form:

$$\begin{aligned} \dot{\mathbf{z}}_i(t) &= \kappa \sum_{j \in \mathcal{N}_i} \operatorname{sgn}(\hat{\mathbf{d}}_{\mathcal{H}}^{(j)}(t) - \hat{\mathbf{d}}_{\mathcal{H}}^{(i)}(t)), \\ \hat{\mathbf{d}}_{\mathcal{H}}^{(i)}(t) &= \mathbf{z}_i(t) + \mathbf{r}_i(t), \end{aligned} \tag{17}$$

with initial condition $\sum_{i=0}^{N-1} \mathbf{z}_i(0) = \mathbf{0}$. $\kappa \in \mathbb{R}$ is a positive design parameter, $\mathbf{z}_i(t) \in \mathbb{R}^{2H}$ represents the internal local state for agent i, $\hat{\mathbf{d}}_{\mathcal{H}}^{(j)}(t)$ is the estimate received by agent i from j who is a graph neighbor, and $\mathbf{r}_i(t) \in \mathbb{R}^{2H}$ is the vector of local reference signals for agent i, defined as

$$\mathbf{r}_i(t) = N \begin{bmatrix} \mathbf{M}_{0,i} \\ \vdots \\ \mathbf{M}_{\frac{H-1}{2},i} \\ \mathbf{M}_{N-\frac{H-1}{2},i} \\ \vdots \\ \mathbf{M}_{N-1,i} \end{bmatrix} \mathbf{p}_i(t). \tag{18}$$

A convergence result for this algorithm is given next.

Proposition 1: Using the algorithm (17) with $\kappa > N \cdot v_{\max}$, $\hat{\mathbf{d}}_{\mathcal{H}}^{(i)}(t)\ \forall i \in \mathcal{N}$ converges to $\mathbf{d}_{\mathcal{H}}(t)$ in finite time.

Proof: Following [19], we consider the dynamics of the reference signals, which we express as $\dot{\mathbf{r}}_i(t) = \mathbf{g}_i(t)$ where $\mathbf{g}_i(t)\ \forall i \in \mathcal{N}$ is measurable and bounded; in particular, due to the linear velocity saturation constraints and every $\mathbf{M}_{l,i}\ \forall l \in \mathcal{H}, \forall i \in \mathcal{N}$ being a rotation matrix, we have $\sup_{t\in[0,\infty)} \|\mathbf{g}_i(t)\|_\infty \leq N \cdot v_{\max}$. Hence, $\kappa > N \cdot v_{\max} \geq \sup_{t\in[0,\infty)} \|\mathbf{g}_i(t)\|_\infty\ \forall i \in \mathcal{N}$. This condition and $\mathcal{G}$ being connected and time-invariant imply, by virtue of Theorem 1 in [19], that $\hat{\mathbf{d}}_{\mathcal{H}}^{(i)}(t)\ \forall i \in \mathcal{N}$ converges to the average of $\mathbf{r}_i(t)$ $\forall i \in \mathcal{N}$ in finite time; i.e., there exists $\mathcal{T} > 0$ such that

$$\begin{aligned} \hat{\mathbf{d}}_{\mathcal{H}}^{(i)}(t) &= \frac{1}{N} \sum_{j=0}^{N-1} \mathbf{r}_j(t) = \frac{1}{N} \sum_{j=0}^{N-1} N \begin{bmatrix} \mathbf{M}_{0,j} \\ \vdots \\ \mathbf{M}_{\frac{H-1}{2},j} \\ \mathbf{M}_{N-\frac{H-1}{2},j} \\ \vdots \\ \mathbf{M}_{N-1,j} \end{bmatrix} \mathbf{p}_j(t) \\ &= \mathbf{M}_{\mathcal{H}} \mathbf{p}(t) = \mathbf{d}_{\mathcal{H}}(t),\ \forall i \in \mathcal{N},\ \forall t \geq \mathcal{T}, \end{aligned} \tag{19}$$

which proves the stated result. ∎

Remark 1: Algorithm (17) is an interesting choice for several reasons: it provides finite-time convergence, it only requires a connected graph and one-hop communication, the size of the managed data ($2H$) is small and independent of N, and only positions (and not their derivatives) are used. The algorithm requires the initial condition $\sum_{i=0}^{N-1} \mathbf{z}_i(0) = \mathbf{0}$, which can be satisfied, e.g., if every agent $i \in \mathcal{N}$ chooses $\mathbf{z}_i(0) = \mathbf{0}$. Note that other dynamic average consensus algorithms guaranteeing finite-time convergence under bounded derivatives of the reference signals could also be used.

B. Gradient-based controller for unicycle agents

Following [15], we propose to use a gradient-based strategy to achieve the control goal $\mathbf{p}(t) \to \mathbf{p}_{\mathcal{H}}(t)$. As explained above, in our strategy each agent uses the estimates of the Fourier descriptors computed with the distributed algorithm in (17). Let us first define the matrix

$$\mathbf{B} = \mathbf{I}_{2N} - \mathbf{A}, \tag{20}$$

which is symmetric and idempotent, and the cost

$$V(\mathbf{p}(t)) = \frac{1}{2}\|\mathbf{p}(t) - \mathbf{p}_{\mathcal{H}}(t)\|^2 = \frac{1}{2}\mathbf{p}(t)^\intercal \mathbf{B} \mathbf{p}(t). \tag{21}$$

Note that $\mathbf{B}$ is positive semidefinite. The negative gradient of the cost $V(\mathbf{p}(t))$ is

$$\mathbf{f}(\mathbf{p}(t)) = -\nabla_{\mathbf{p}} V(\mathbf{p}(t)) = -\mathbf{B}\mathbf{p}(t) = \mathbf{p}_{\mathcal{H}}(t) - \mathbf{p}(t), \tag{22}$$

where $\mathbf{f}(\mathbf{p}(t)) = [\mathbf{f}_0(\mathbf{p}(t))^\intercal, \ldots, \mathbf{f}_{N-1}(\mathbf{p}(t))^\intercal]^\intercal$, and for every individual agent $i \in \mathcal{N}$ we have

$$\mathbf{f}_i(\mathbf{p}(t)) = -\nabla_{\mathbf{p}_i} V(\mathbf{p}(t)) = \mathbf{p}_{\mathcal{H},i}(t) - \mathbf{p}_i(t). \tag{23}$$

Recall that $\mathbf{p}_{\mathcal{H},i}(t)$ can be computed from the vector of Fourier descriptors $\mathbf{d}_{\mathcal{H}}(t)$ as expressed in (16). Agent i does not have direct access to the true vector $\mathbf{d}_{\mathcal{H}}(t)$ but can estimate it via (17). In particular, agent i can compute

$$\hat{\mathbf{p}}_{\mathcal{H},i}^{(i)}(t) = \frac{1}{N} \left[\mathbf{M}_{0,i}, \ldots, \mathbf{M}_{\frac{H-1}{2},i}, \mathbf{M}_{N-\frac{H-1}{2},i}, \ldots, \mathbf{M}_{N-1,i}\right] \hat{\mathbf{d}}_{\mathcal{H}}^{(i)}(t). \tag{24}$$

If the agents obeyed single-integrator dynamics, one could propose the following gradient-based control law:

$$\dot{\mathbf{p}}_i(t) = \hat{\mathbf{f}}_i^{(i)}(\mathbf{p}(t)) = \hat{\mathbf{p}}_{\mathcal{H},i}^{(i)}(t) - \mathbf{p}_i(t). \tag{25}$$

Then, the control law we propose for unicycle agents is based on adapting the single-integrator one as done in [20, eq. 12]:

$$v_i(t) = \operatorname{sat}_{v_i}\Big([\cos(\theta_i(t)), \sin(\theta_i(t))]\, \hat{\mathbf{f}}_i^{(i)}(\mathbf{p}(t))\Big), \tag{26}$$

$$\omega_i(t) = \operatorname{sat}_{\omega_i}\Big([-\sin(\theta_i(t)), \cos(\theta_i(t))]\, \hat{\mathbf{f}}_i^{(i)}(\mathbf{p}(t))\Big). \tag{27}$$

This control law follows the general approach proposed in [20] for modifying a single-integrator gradient control law to take into account motion constraints, while retaining the convergence properties of the original law. We analyze our control law next.

Theorem 1: Under the action of the control law (26), (27), it holds that $\mathbf{p}(t) \to \mathbf{p}_{\mathcal{H}}(t)$ as $t \to \infty$, i.e., the agents converge globally asymptotically to a configuration whose descriptors are zero for all indices outside $\mathcal{H}$.

Proof: First, note that finite-time escapes of $\mathbf{p}(t)$ are not possible under (26), (27) because the linear velocity is bounded by the saturation constraints. Hence, $\mathbf{p}(t)$ remains bounded until the convergence of the estimator (17) which, from Proposition 1, occurs at a finite time instant $\mathcal{T}$. For $t \geq \mathcal{T}$ we have $\hat{\mathbf{d}}_{\mathcal{H}}^{(i)}(t) = \mathbf{d}_{\mathcal{H}}(t)$, $\hat{\mathbf{p}}_{\mathcal{H},i}^{(i)}(t) = \mathbf{p}_{\mathcal{H},i}(t)$, and $\hat{\mathbf{f}}_i^{(i)}(\mathbf{p}(t)) = \mathbf{f}_i(\mathbf{p}(t))\ \forall i \in \mathcal{N}$, and hence the single-integrator control law from (25) is $\dot{\mathbf{p}}(t) = \mathbf{f}(\mathbf{p}(t))\ \forall t \geq \mathcal{T}$. We study the system for $t \geq \mathcal{T}$ next.

Let us define the error vector $\mathbf{e}(t) = \mathbf{p}(t) - \mathbf{p}_{\mathcal{H}}(t) = \mathbf{B}\mathbf{p}(t)$. Notice $V(\mathbf{e}(t)) = (1/2)\|\mathbf{e}(t)\|^2$. We next analyze the convergence of the modified control law (26), (27) by examining a set of four conditions for the gradient control law $\dot{\mathbf{p}}(t) = \mathbf{f}(\mathbf{p}(t))$ [20, Assumption 1]: 1) $V(\mathbf{e}(t)) = (1/2)\|\mathbf{e}(t)\|^2$ is a Lyapunov function whose level sets $\Omega(r) = \{\mathbf{e} : V(\mathbf{e}) \leq r\}$ are compact for any $r \geq 0$; 2) As $\mathbf{f}(\mathbf{p}(t)) = -\mathbf{e}(t)$, we have $\mathbf{e}(t) = \mathbf{0} \Leftrightarrow \mathbf{f}(\mathbf{p}(t)) = \mathbf{0}$ everywhere; 3) $\|\partial\mathbf{e}/\partial\mathbf{p}\| = \|\mathbf{B}\|$ and $\|\mathbf{f}(\mathbf{p}(t))\| = \|\mathbf{e}(t)\|$ are bounded for bounded $\|\mathbf{e}(t)\|$; 4) $\mathbf{f}(\mathbf{p}(t)) = -\mathbf{e}(t) = -\mathbf{B}\mathbf{p}(t)$ is continuous in $\mathbf{e}$, and uniformly continuous in $\mathbf{p}$ since it is a linear transformation.

As noted in [20], these conditions imply the gradient control law $\dot{\mathbf{p}}(t) = \mathbf{f}(\mathbf{p}(t))$ is globally convergent due to LaSalle's invariance principle and they ensure, from Theorem 4 in [20], that under control law (26), (27) it holds globally that $\mathbf{e}(t) \to \mathbf{0}$, i.e., $\mathbf{p}(t) \to \mathbf{p}_{\mathcal{H}}(t)$, as $t \to \infty$. ■

Remark 2: With our approach, the agents converge to a static configuration, as their velocities vanish when the gradient is zero. The approach does not control the specific shape of the curve, which depends on the initial conditions and on the system dynamics. The achieved closed curve is an ellipse if $H = 3$. If $H > 3$, the achieved closed curve may be simple (i.e., with no self intersections) or self-intersecting. A simple curve is a suitable solution for standard enclosing behaviors, while a self-intersecting curve makes the team's shape more flexible and can be interesting in some applications; for, e.g., creating multiple adjacent enclosed areas. Also, our formation specification allows descriptors of any value for the frequencies in $\mathcal{H}$, and therefore it is possible to achieve degenerate curves (e.g., degenerate ellipses if $H = 3$).

Remark 3: As $\mathbf{p}(t)$ and $\mathbf{p}_{\mathcal{H}}(t)$ have the same zero-frequency content, they have the same centroid, since $(1/N)\sum_{i\in\mathcal{N}} \mathbf{p}_i(t) = (1/N)\mathbf{d}_0(t)$ from (6). Also, defining the scale (i.e., size relative to the centroid) as follows:

$$s(\mathbf{p}(t)) = \frac{1}{N}\sum_{i\in\mathcal{N}} \left\| \mathbf{p}_i(t) - \frac{1}{N}\sum_{j\in\mathcal{N}} \mathbf{p}_j(t) \right\|^2, \tag{28}$$

then for a given $\mathbf{p}(t)$, $s(\mathbf{p}_{\mathcal{H}}(t))$ is less than or equal to $s(\mathbf{p}(t))$, as studied in [15]. Another interesting fact from [15] is that $\mathbf{p}_{\mathcal{H}}(t)$ is time-invariant under a single-integrator gradient control $\dot{\mathbf{p}}(t) = \mathbf{f}(\mathbf{p}(t))$. The behavior in this respect is similar with our unicycle control, as it is gradient-based; this is visible in our simulations and implies there is no persistent downward drift of the scale. The scale may be kept under control in practice by the constraints of a higher-level task: e.g., maintaining lower-bounded agent-to-agent and agent-to-target distances in a target enclosing task. Note that our approach does not avoid interagent collisions. To address this issue, one could incorporate a collision avoidance strategy; e.g., exploiting control barrier functions [25]. While this would not guarantee the maintenance of our controller's convergence properties, it is a widespread practical solution.

C. Combining sets of frequencies

In some scenarios, it can be interesting to use two different sets of low frequencies, $\mathcal{H}_1$ with H_1 elements, and $\mathcal{H}_2$ with $H_2 > H_1$ elements. To accomplish this, we exploit a linear combination of two (one per set) gradient-based single-integrator terms like the one in (25). The team will then eventually reach a low-frequency formation consistent with $\mathcal{H}_1$. The intuitive reason (formalized below) is that $\mathcal{H}_1 \subset \mathcal{H}_2$ and thus, combined motions toward configurations consistent with the two sets finally converge to a configuration consistent with the smaller of the two. However, instead of moving directly toward the final formation, the team will remain close to a low-frequency formation consistent with $\mathcal{H}_2$ during the transient interval. This is interesting as it makes the transition more gradual and overall provides a stronger low-frequency formation-keeping behavior.

Following developments presented above, we can define matrices $\mathbf{A}_1$ for $\mathcal{H}_1$ and $\mathbf{A}_2$ for $\mathcal{H}_2$, with $\mathbf{p}_{\mathcal{H}_1}(t) = \mathbf{A}_1\mathbf{p}(t)$ and $\mathbf{p}_{\mathcal{H}_2}(t) = \mathbf{A}_2\mathbf{p}(t)$ being the desired formations associated with $\mathcal{H}_1$ and $\mathcal{H}_2$ respectively. We also define $\mathbf{B}_1 = \mathbf{I}_{2N} - \mathbf{A}_1$, $\mathbf{B}_2 = \mathbf{I}_{2N} - \mathbf{A}_2$. Note that once again $\mathbf{B}_1$ and $\mathbf{B}_2$ are real symmetric positive semidefinite. Let us now define $\bar{\mathbf{B}} = \alpha_1\mathbf{B}_1 + \alpha_2\mathbf{B}_2$, with α_1, α_2 being two real positive scalars that represent the weight of the control terms associated with $\mathcal{H}_1$ and $\mathcal{H}_2$ respectively. Choosing either $\alpha_1 = 0$ or $\alpha_2 = 0$ one obtains the controller of Sec. III-B. Notice that $\bar{\mathbf{B}}$ is real symmetric positive semidefinite. We now define a corresponding cost as

$$\bar{V}(\mathbf{p}(t)) = (1/2)\mathbf{p}(t)^\intercal\bar{\mathbf{B}}\mathbf{p}(t). \tag{29}$$

We can define a single-integrator control law based on the negative gradient of $\bar{V}$ which is

$$\begin{aligned}\bar{\mathbf{f}}(\mathbf{p}(t)) &= -\nabla_{\mathbf{p}}\bar{V}(\mathbf{p}(t)) = -\bar{\mathbf{B}}\mathbf{p}(t)) \\ &= \alpha_1(\mathbf{p}_{\mathcal{H}_1}(t) - \mathbf{p}(t)) + \alpha_2(\mathbf{p}_{\mathcal{H}_2}(t) - \mathbf{p}(t)),\end{aligned} \tag{30}$$

where $\bar{\mathbf{f}}(\mathbf{p}(t)) = [\bar{\mathbf{f}}_0(\mathbf{p}(t))^\intercal, \ldots, \bar{\mathbf{f}}_{N-1}(\mathbf{p}(t))^\intercal]^\intercal$ and we have for every individual agent $i \in \mathcal{N}$ that

$$\begin{aligned}\bar{\mathbf{f}}_i(\mathbf{p}(t)) &= -\nabla_{\mathbf{p}_i}\bar{V}(\mathbf{p}(t)) \\ &= \alpha_1(\mathbf{p}_{\mathcal{H}_1,i}(t) - \mathbf{p}_i(t)) + \alpha_2(\mathbf{p}_{\mathcal{H}_2,i}(t) - \mathbf{p}_i(t)).\end{aligned} \tag{31}$$

Agent i can obtain an estimate $\hat{\mathbf{d}}^{(i)}_{\mathcal{H}_2}(t)$ by means of algorithm (17). As $\mathcal{H}_1 \subset \mathcal{H}_2$, this directly gives $\hat{\mathbf{d}}^{(i)}_{\mathcal{H}_1}(t)$ as well. From this, agent i can obtain $\hat{\mathbf{p}}^{(i)}_{\mathcal{H}_1,i}(t)$ and $\hat{\mathbf{p}}^{(i)}_{\mathcal{H}_2,i}(t)$ as in (24). Then, we define the following gradient-based control law:

$$\dot{\mathbf{p}}_i(t) = \hat{\bar{\mathbf{f}}}^{(i)}_i(\mathbf{p}(t)) = \alpha_1(\hat{\mathbf{p}}^{(i)}_{\mathcal{H}_1,i}(t) - \mathbf{p}_i(t)) + \alpha_2(\hat{\mathbf{p}}^{(i)}_{\mathcal{H}_2,i}(t) - \mathbf{p}_i(t)). \tag{32}$$

We propose a unicycle control law as in (26), (27); i.e., we adapt the single-integrator control law (32) as follows:

$$v_i(t) = \mathrm{sat}_{v_i}\Big([\cos(\theta_i(t)), \sin(\theta_i(t))]\hat{\bar{\mathbf{f}}}^{(i)}_i(\mathbf{p}(t))\Big), \tag{33}$$

$$\omega_i(t) = \mathrm{sat}_{\omega_i}\Big([-\sin(\theta_i(t)), \cos(\theta_i(t))]\hat{\bar{\mathbf{f}}}^{(i)}_i(\mathbf{p}(t))\Big). \tag{34}$$

Theorem 2: Under the action of the control law (33), (34), it holds that $\mathbf{p}(t) \to \mathbf{p}_{\mathcal{H}_1}(t)$ as $t \to \infty$, i.e., the agents converge globally asymptotically to a configuration whose descriptors are zero for all indices outside $\mathcal{H}_1$.

Proof: As in Theorem 1, finite-time escapes of $\mathbf{p}(t)$ under (33), (34) cannot occur due to the velocity saturation

constraints, and Proposition 1 ensures there is a finite $\mathcal{T} > 0$ at which estimator (17) has converged, i.e., $\forall t \geq \mathcal{T}$ $\hat{\bar{\mathbf{f}}}_i^{(i)}(\mathbf{p}(t)) = \bar{\mathbf{f}}_i(\mathbf{p}(t))$ in (33), (34) and the single-integrator control law from (32) is $\dot{\mathbf{p}}(t) = \bar{\mathbf{f}}(\mathbf{p}(t))$. We analyze the system for $t \geq \mathcal{T}$ next. Let $\bar{\mathbf{e}}(t) = \bar{\mathbf{B}}^{1/2}\mathbf{p}(t)$ be the error vector where $\bar{\mathbf{B}}^{1/2}$ is the real symmetric positive semidefinite square root of $\bar{\mathbf{B}}$. Notice $\bar{V}(\bar{\mathbf{e}}(t)) = (1/2)\|\bar{\mathbf{e}}(t)\|^2$. We study again the four conditions in Assumption 1 of [20] for $\dot{\mathbf{p}}(t) = \bar{\mathbf{f}}(\mathbf{p}(t))$: 1) $\bar{V}(\bar{\mathbf{e}}(t)) = (1/2)\|\bar{\mathbf{e}}(t)\|^2$ is a Lyapunov function whose level sets $\bar{\Omega}(r) = \{\bar{\mathbf{e}} : \bar{V}(\bar{\mathbf{e}}) \leq r\}$ are compact for any $r \geq 0$; 2) As $\bar{\mathbf{f}}(\mathbf{p}(t)) = -\bar{\mathbf{B}}^{1/2}\bar{\mathbf{e}}(t)$, we have $\bar{\mathbf{e}}(t) = \mathbf{0} \Rightarrow \bar{\mathbf{f}}(\mathbf{p}(t)) = \mathbf{0}$ and $\bar{\mathbf{f}}(\mathbf{p}(t)) = \mathbf{0} \Rightarrow \bar{V}(\bar{\mathbf{e}}(t)) = 0 \Rightarrow \bar{\mathbf{e}}(t) = \mathbf{0}$ everywhere; 3) $\|\partial\bar{\mathbf{e}}/\partial\mathbf{p}\| = \|\bar{\mathbf{B}}^{1/2}\|$ and $\|\bar{\mathbf{f}}(\mathbf{p}(t))\| = \|\bar{\mathbf{B}}^{1/2}\bar{\mathbf{e}}(t)\|$ are bounded for bounded $\|\bar{\mathbf{e}}(t)\|$; 4) $\bar{\mathbf{f}}(\mathbf{p}(t)) = -\bar{\mathbf{B}}^{1/2}\bar{\mathbf{e}}(t) = -\bar{\mathbf{B}}\mathbf{p}(t)$ is continuous in $\bar{\mathbf{e}}$, and uniformly continuous in $\mathbf{p}$ since it is a linear transformation.

Similarly to Theorem 1, these conditions imply that the gradient control law $\dot{\mathbf{p}}(t) = \bar{\mathbf{f}}(\mathbf{p}(t))$ is globally convergent by virtue of LaSalle's invariance principle and they guarantee, from Theorem 4 in [20], that under the control law (33), (34) it holds globally that $\bar{\mathbf{e}}(t) \to \mathbf{0}$ and hence $\bar{V} = (1/2)\mathbf{p}(t)^\intercal\bar{\mathbf{B}}\mathbf{p}(t) \to 0$ as $t \to \infty$. Recall that $\mathbf{B}_1$, $\mathbf{B}_2$ are real symmetric positive semidefinite, and α_1, α_2 are positive. Using well-known properties of real symmetric positive semidefinite matrices, we have

$$\begin{aligned}&\mathbf{p}(t)^\intercal\bar{\mathbf{B}}\mathbf{p}(t) = 0 \Rightarrow \alpha_1\mathbf{p}(t)^\intercal\mathbf{B}_1\mathbf{p}(t) + \alpha_2\mathbf{p}(t)^\intercal\mathbf{B}_2\mathbf{p}(t) = 0\\ &\Rightarrow \mathbf{B}_1\mathbf{p}(t) = \mathbf{0} \text{ and } \mathbf{B}_2\mathbf{p}(t) = \mathbf{0}. \qquad (35)\end{aligned}$$

This directly implies the condition $\mathbf{p}(t) = \mathbf{p}_{\mathcal{H}_1}(t) = \mathbf{p}_{\mathcal{H}_2}(t)$. Recalling that $\mathcal{H}_1 \subset \mathcal{H}_2$, the interpretation of this condition is that the descriptors of $\mathbf{p}(t)$ for frequencies outside $\mathcal{H}_2$ are zero (due to $\mathbf{p}(t) = \mathbf{p}_{\mathcal{H}_2}(t)$), and the descriptors for frequencies in $\mathcal{H}_2$ but not in $\mathcal{H}_1$ are zero as well (due to $\mathbf{p}(t) = \mathbf{p}_{\mathcal{H}_1}(t)$). The condition clearly reduces to $\mathbf{p}(t) = \mathbf{p}_{\mathcal{H}_1}(t)$, which concludes the proof. ■

IV. Simulation Results

We present results from several numerical examples run in MATLAB. Videos for these and other examples are also available via the provided link[1]. In all the examples, the graph $\mathcal{G}$ has a ring topology such that $\mathcal{N}_0 = \{1, N-1\}$, $\mathcal{N}_{N-1} = \{N-2, 0\}$, and $\mathcal{N}_i = \{i-1, i+1\}$ for the other $i \in \mathcal{N}$. The saturation limits are $v_{f_i} = v_{b_i} = 0.5$ m/s and $\omega_{l_i} = \omega_{r_i} = \pi/4$ rad/s $\forall i \in \mathcal{N}$. The estimator and the controller run at 10 kHz and 100 Hz, respectively. In our first example, we consider $N = 8$ agents and we take $H = 3$ and $\kappa = 10 \cdot N \cdot v_{\max}$. The results in Fig. 2 show the finite-time convergence of the estimation of the descriptors and the asymptotic convergence of the team to a discretized ellipse.

For the remaining examples, we use $N = 20$ and $\kappa = 20 \cdot N \cdot v_{\max}$, choosing $H_1 = 3$, $H_2 = 5$ to test the combination of frequency sets (Sec. III-C). We do three runs from an identical initial configuration with: 1) $\alpha_1 = 0.1$, $\alpha_2 = 0$, 2) $\alpha_1 = 0.1$, $\alpha_2 = 1$, 3) $\alpha_1 = 0$, $\alpha_2 = 0.1$. As shown in Fig. 3, the expected convergence behavior is obtained in all cases. Comparing cases 1) and 2) at $t = 8$ s, in 2) the formed curve is clearly smoother, indicating that the agents stay on a lower-frequency curve during the transient interval. The time plots show that when $\alpha_2 = 1$, the high-frequency descriptors (i.e., those for the set $\mathcal{N} \setminus \mathcal{H}_2$) vanish more rapidly.

[1]https://www.youtube.com/playlist?list=PLp_Aa-IfaBfHC3fF8tL5ShGV9H1PoDFbA

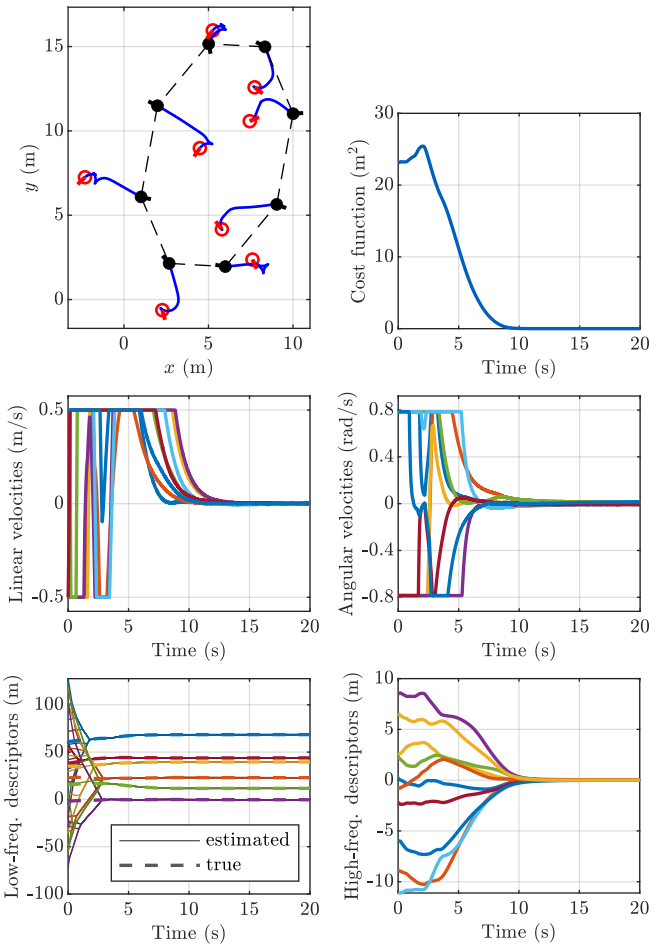

Fig. 2. Results for the 8-agent simulation example. Top left: agents' paths (blue solid lines), initial positions (red hollow circles, headings as red line segments), and final positions (black solid circles, headings as black line segments); black dashed lines join the final positions to represent the outline of the final curve. Top right: cost function V. Middle left: linear velocities. Middle right: angular velocities. Bottom left: estimated values of all the components of $\mathbf{d}_{\mathcal{H}}(t)$ from the algorithm (17) and true values of these components. Bottom right: values of all the components of the descriptors for the frequencies outside $\mathcal{H}$, i.e., the components of $\mathbf{d}_k(t)$ for $k \in \mathcal{N} \setminus \mathcal{H}$.

V. Conclusion

This paper has presented an estimation-based control approach that enables a useful distributed formation-keeping behavior for multiagent teams by exploiting Fourier descriptors. In terms of future work, we would like to explore how to gain finer control on the properties of the formation by, e.g., keeping the values of the low-frequency descriptors in certain ranges. Another direction worth pursuing is using different dynamic models, both for the estimator and for the controller.

References

[1] J. Alonso-Mora, S. Baker, and D. Rus, "Multi-robot formation control and object transport in dynamic environments via constrained optimization," *Int. J. Robot. Res.*, vol. 36, no. 9, pp. 1000–1021, 2017.

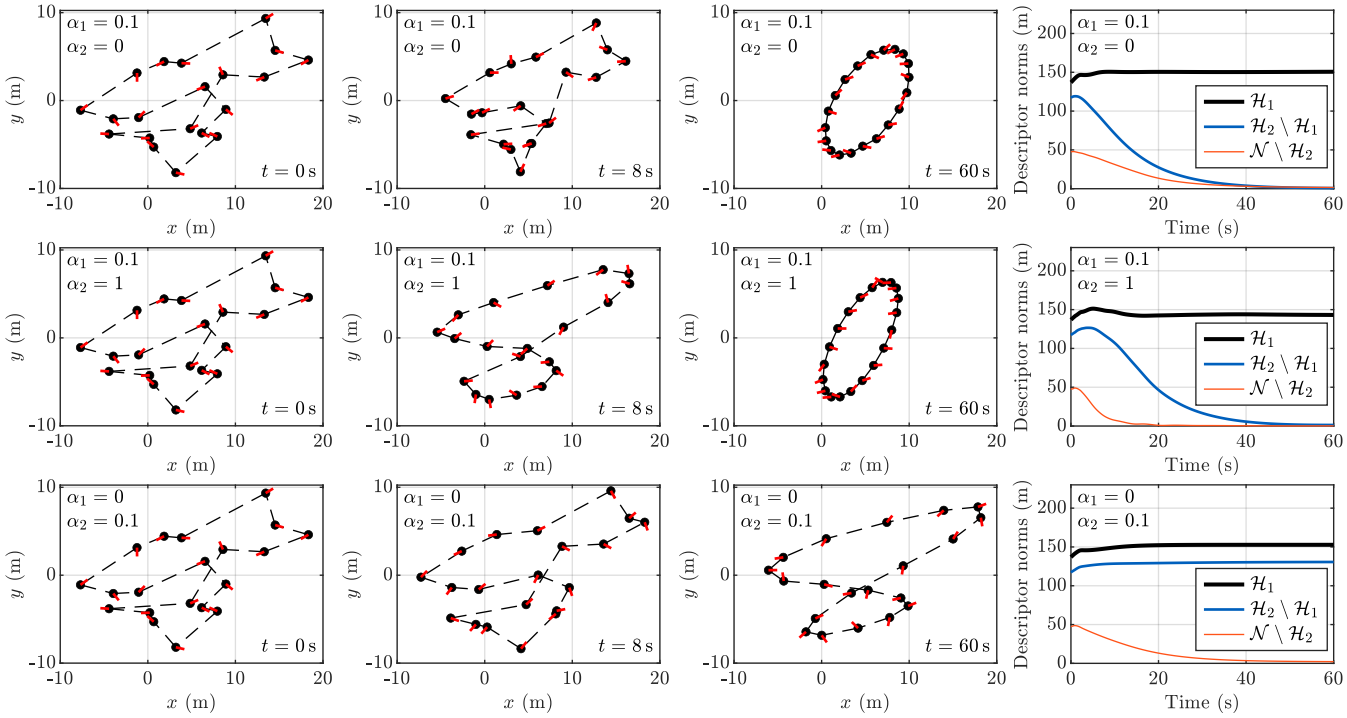

Fig. 3. Results for the 20-agent simulation examples. Snapshots of the team's configuration with the corresponding α parameters and time stamps are shown. Positions are marked by black circles and headings by red line segments, and dashed black lines join neighboring agents for the considered sequence. In the rightmost column, the Euclidean norms of the vectors containing the descriptors for frequencies in $\mathcal{H}_1$, $\mathcal{H}_2 \setminus \mathcal{H}_1$, and $\mathcal{N} \setminus \mathcal{H}_2$ are shown.

[2] G. López-Nicolás, M. Aranda, and Y. Mezouar, "Adaptive multirobot formation planning to enclose and track a target with motion and visibility constraints," *IEEE Trans. Robot.*, vol. 36, no. 1, pp. 142–156, 2020.

[3] L. Krick, M. E. Broucke, and B. A. Francis, "Stabilisation of infinitesimally rigid formations of multi-robot networks," *Int. J. Control*, vol. 82, no. 3, pp. 423–439, 2009.

[4] F. Mehdifar, C. P. Bechlioulis, F. Hashemzadeh, and M. Baradarannia, "Prescribed performance distance-based formation control of multi-agent systems," *Automatica*, vol. 119, p. 109086, 2020.

[5] W. Ren, "Consensus strategies for cooperative control of vehicle formations," *IET Control Theory Appl.*, vol. 1, no. 2, pp. 505–512, 2007.

[6] M. Aranda, R. Aragüés, and G. López-Nicolás, "Combined leaderless control of translational, shape-preserving, and affine multirobot formations," *IEEE Robot. Autom. Lett.*, vol. 8, no. 11, pp. 7567–7574, 2023.

[7] S. Zhao and D. Zelazo, "Bearing rigidity and almost global bearing-only formation stabilization," *IEEE Trans. Automat. Contr.*, vol. 61, no. 5, pp. 1255–1268, 2016.

[8] M. H. Trinh, S. Zhao, Z. Sun, D. Zelazo, B. D. O. Anderson, and H.-S. Ahn, "Bearing-based formation control of a group of agents with leader-first follower structure," *IEEE Trans. Autom. Control*, vol. 64, no. 2, pp. 598–613, 2019.

[9] M. Aranda, G. López-Nicolás, C. Sagüés, and Y. Mezouar, "Formation control of mobile robots using multiple aerial cameras," *IEEE Trans. Robot.*, vol. 31, no. 4, pp. 1064–1071, 2015.

[10] D. Li, S. S. Ge, W. He, G. Ma, and L. Xie, "Multilayer formation control of multi-agent systems," *Automatica*, vol. 109, p. 108558, 2019.

[11] N. Michael and V. Kumar, "Controlling shapes of ensembles of robots of finite size with nonholonomic constraints," in *Robot.: Sci. Syst. IV*. The MIT Press, 2009, pp. 41–48.

[12] C. J. Stamouli, C. P. Bechlioulis, and K. J. Kyriakopoulos, "Multi-agent formation control based on distributed estimation with prescribed performance," *IEEE Robot. Automat. Lett.*, vol. 5, no. 2, pp. 2929–2934, 2020.

[13] G. Fedele, L. D'Alfonso, and A. Bono, "A discrete-time model for swarm formation with coordinates coupling matrix," *IEEE Control Syst. Lett.*, vol. 4, no. 4, pp. 1012–1017, 2020.

[14] G. C. Maffettone, A. Boldini, M. Di Bernardo, and M. Porfiri, "Continuification control of large-scale multiagent systems in a ring," *IEEE Control Syst. Lett.*, vol. 7, pp. 841–846, 2023.

[15] M. Aranda, "Formation control on planar closed curves using Fourier descriptors," *IEEE Control Syst. Lett.*, vol. 7, pp. 3391–3396, 2023.

[16] S. Evren and M. Unel, "Planar formation control of swarm robots using dynamical elliptic Fourier descriptors," *Trans. Inst. Meas. Control*, vol. 37, no. 5, pp. 661–671, 2015.

[17] B. Zhang et al., "Fourier-based multi-agent formation control to track evolving closed boundaries," *IEEE Trans. Circuits Syst. I: Regul. Pap.*, vol. 70, no. 11, pp. 4549–4559, 2023.

[18] R. Aldana-López, D. Gómez-Gutiérrez, R. Aragüés, and C. Sagüés, "Dynamic consensus with prescribed convergence time for multileader formation tracking," *IEEE Control Syst. Lett.*, vol. 6, pp. 3014–3019, 2022.

[19] F. Chen, Y. Cao, and W. Ren, "Distributed average tracking of multiple time-varying reference signals with bounded derivatives," *IEEE Trans. Autom. Control*, vol. 57, no. 12, pp. 3169–3174, 2012.

[20] S. Zhao, D. V. Dimarogonas, Z. Sun, and D. Bauso, "A general approach to coordination control of mobile agents with motion constraints," *IEEE Trans. Autom. Control*, vol. 63, no. 5, pp. 1509–1516, 2018.

[21] J. G. Proakis and D. G. Manolakis, *Digital signal processing: Principles, algorithms, and applications (3rd ed.)*. Prentice Hall, 1996.

[22] R. C. González and R. E. Woods, *Digital image processing, 3rd Edition*. Pearson Education, 2008.

[23] D. Navarro-Alarcon and Y.-H. Liu, "Fourier-based shape servoing: A new feedback method to actively deform soft objects into desired 2-D image contours," *IEEE Trans. Robot.*, vol. 34, no. 1, pp. 272–279, 2018.

[24] S. S. Kia, B. Van Scoy, J. Cortes, R. A. Freeman, K. M. Lynch, and S. Martinez, "Tutorial on dynamic average consensus: The problem, its applications, and the algorithms," *IEEE Control Syst. Mag.*, vol. 39, no. 3, pp. 40–72, 2019.

[25] L. Wang, A. D. Ames, and M. Egerstedt, "Safety barrier certificates for collisions-free multirobot systems," *IEEE Trans. Robot.*, vol. 33, no. 3, pp. 661–674, 2017.